AGU PUBLICATIONS

Water Resources Research

RESEARCH ARTICLE
10.1002/2013WR015236

Special Section:
Eco-hydrology of Semiarid Environments: Confronting Mathematical Models with Ecosystem Complexity

A dynamical system perspective on plant hydraulic failure

Stefano Manzoni[1,2], Gabriel Katul[3,4], and Amilcare Porporato[3,4]

[1]Department of Physical Geography and Quaternary Geology, Stockholm University, Stockholm, Sweden, [2]Departments of Crop Production Ecology and Ecology, Swedish University of Agricultural Sciences, Uppsala, Sweden, [3]Nicholas School of the Environment, Duke University, Durham, North Carolina, USA, [4]Department of Civil and Environmental Engineering, Duke University, Durham, North Carolina, USA

Key Points:
- Plant hydraulic failure is interpreted as a dynamic catastrophe
- Viable and desiccated states emerge as alternative steady states
- Low moisture and high VPD trigger desiccation in previously stressed plants

Correspondence to:
S. Manzoni,
stefano.manzoni@natgeo.su.se

Citation:
Manzoni, S., G. Katul, and A. Porporato (2014), A dynamical system perspective on plant hydraulic failure, *Water Resour. Res.*, *50*, 5170–5183, doi:10.1002/2013WR015236.

Received 27 DEC 2013
Accepted 4 JUN 2014
Accepted article online 9 JUN 2014
Published online 27 JUN 2014

Abstract Photosynthesis is governed by leaf water status that depends on the difference between the rates of transpiration and water supply from the soil and through the plant xylem. When transpiration increases compared to water supply, the leaf water potential reaches a more negative equilibrium, leading to water stress. Both high atmospheric vapor pressure deficit and low soil moisture increase the water demand while decreasing the supply due to lowered soil-to-root conductance and xylem cavitation. Therefore, dry conditions may eventually reduce the leaf water potential to the point of collapsing the plant hydraulic system. This "hydraulic failure" is shown to correspond to a fold bifurcation where the environmental parameters (vapor pressure deficit and soil moisture) trigger the loss of a physiologically sustainable equilibrium. Using a minimal plant hydraulic model, coordination among plant hydraulic traits is shown to result in increased resilience to environmental stresses, thereby impeding hydraulic failure unless hydraulic traits deteriorate due to prolonged water shortage or other damages.

1. Introduction

Water is transported from soil to leaves along a gradient in water potential sustained by evaporation through stomatal pores [*Jones*, 1992; *Rodriguez-Iturbe and Porporato*, 2004; *van den Honert*, 1948]. This flow depends on how efficiently soil and xylem tissues transport water (i.e., soil hydraulic conductivity and xylem conductance, respectively), how fast water is allowed to exit the leaves through evaporation (stomatal conductance), and how much water can be stored and released from plant tissues (stem and leaf hydraulic capacitances). These three factors interact with the boundary conditions imposed by the soil water potential, and the water vapor pressure deficit (D) and aerodynamic conductance in the atmosphere. Most importantly, many of these factors depend on plant water status [*Jones*, 1992; *Manzoni et al*., 2013b], which may lead to sudden dynamical shifts in the functioning point of the hydraulic system. In the most extreme case, the evaporative demand cannot be met by water supply from the soil, resulting in embolism of the xylem. If refilling cannot occur due to persistently dry conditions or limited resources [for a discussion on refilling mechanisms see *Zwieniecki and Holbrook*, 2009], irreversible damage may ensue, possibly leading to mortality [*Allen et al*., 2010; *Martinez-Vilalta and Pinol*, 2002; *McDowell et al*., 2008].

Within the plant xylem water flows under tension, overcoming viscous friction, with a reduction of the flow rate when cavitation ensues [*Tyree and Sperry*, 1988]. Thus the hydraulic conductance of the xylem depends on the water status of the tissues, but also varies at longer time scales following intense water stress events [*Anderegg et al*., 2013]. As the leaf water potential decreases because of increased vapor pressure deficit (D) in the atmosphere or lower soil moisture, xylem water potential also decreases, causing a reduction in xylem conductance due to cavitation and air embolism. A decreased conductance, however, worsens the water status by steepening the water potential gradient [*Tyree and Sperry*, 1988]. While under mild water stress this process is ameliorated by refilling overnight, under persistently dry conditions it might be reinforced, leading to long-term damages. This positive feedback is often named "runaway embolism" [*Meinzer et al*., 2008; *Nardini and Salleo*, 2000], "runaway cavitation" [*Hölttä et al*., 2009; *Tyree and Sperry*, 1988], or "hydraulic failure" [*Brodribb and Cochard*, 2009; *McDowell et al*., 2008].

To avoid or postpone hydraulic failure and associated damages related to partial loss of leaf area or distal branches or even death [*Anderegg et al*., 2013; *Martinez-Vilalta and Pinol*, 2002; *McDowell et al*., 2008], plants strive to maintain a safety margin by reducing the water potential gradient from the soil to the leaves.

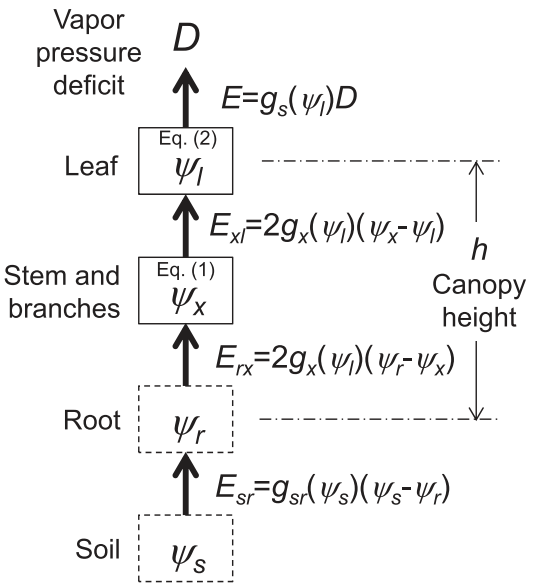

Figure 1. Model scheme showing the water storage compartments (solid boxes, equations (1) and (2)), nodes (dashed boxes), and fluxes (arrows). The xylem storage pool is located at half the canopy height, so that the partial xylem conductances controlling the fluxes in and out of ψ_x are twice the total xylem conductance g_x; nevertheless, xylem conductance is conservatively assumed to depend on the most negative water potential in the plant, i.e., ψ_l.

Different strategies are adopted by plants to decrease this gradient and control cavitation, depending on the time scale of the dry period. At seasonal to ontogenetic time scales, decreasing the leaf to sapwood area ratio improves the plant water status [*Magnani et al*., 2002; *Maseda and Fernandez*, 2006]. At shorter time scales that are of interest here (from subdaily fluctuations in vapor pressure deficit to daily-to-monthly changes in soil moisture), stomatal closure effectively lowers the evaporation rate from the leaves. The rate of stomatal closure as water potential declines controls how much transpiration is reduced and thus how effectively cavitation can be prevented [*McDowell et al*., 2008]. In turn, lowered leaf water potential due to declining xylem conductance triggers stomatal closure [*Buckley*, 2005].

From a dynamical system perspective, hydraulic failure resembles the occurrence of a "catastrophe" in the sense of *Thom* [1975] and *Zeeman* [1976], in which the number of equilibrium states of the system is suddenly reduced as control parameters change. In the case of plants, high D and low soil water potential may cause this collapse, driving the plant system from hydrated to water-stressed conditions. Conditions of either enhanced water demand or reduced supply are more frequent in semiarid ecosystems, although they also occur in more mesic systems. This sudden loss of hydraulic function shifts the plant to an alternative, desiccated steady state, qualitatively similar to ecosystem-level tipping points [*Runyan et al*., 2012; *Scheffer et al*., 2001]. Catastrophe theory offers a general framework to link the discontinuities associated with hydraulic failure to the control parameters (environmental conditions and plant hydraulic traits) that trigger or prevent the occurrence of "hydraulic catastrophes." This alternative perspective on plant hydraulic dynamics frames the scope of this contribution.

Here a simplified analytical model of water transport in the soil-plant-atmosphere system is employed to compute the water potential levels at which a steady transpiration rate is maintained (i.e., the equilibrium points of the plant dynamical system). Two main questions are addressed: (i) What is hydraulic failure from a catastrophe theory perspective? and (ii) How do soil moisture and D (independently or in concert) trigger a state shift from one equilibrium point to another?

2. A Dynamical System Model of Water Flow in Plants

As shown in Figure 1, the soil-plant-atmosphere system may be described as a discrete sequence of resistances linking the soil (at water potential ψ_s) to the roots (ψ_r), the stem and branches (ψ_x), and the leaves (ψ_l). The canopy exchanges water vapor with the atmosphere, characterized by a vapor pressure deficit D [e.g., *Manzoni et al*., 2013b; *Novick et al*., 2009; *Whitehead et al*., 1984]. This representation is simpler than other plant hydraulic models but retains the essential processes and analytically links few control variables to the onset of hydraulic failure (see section 4.1 for a comparison with other approaches).

The model is based on two plant storage compartments (woody tissues and leaves) connected to the soil and the atmosphere through a series of conductances (symbols are explained in Figure 1). While this framework is general, the focus here is on trees, for which hydraulic traits are better characterized than for herbaceous species. Water storage is expressed as a volume of water per unit ground area and fluxes as water depth exchanged per unit time. The mass balance equation for water storage in the woody compartments can be written as

$$C_x \frac{d\psi_x}{dt} = E_{rx} - E_{xl} = 2g_x(\psi_l)(\psi_r - 2\psi_x + \psi_l), \quad (1)$$

where C_x is the xylem hydraulic capacitance, i.e., the relative change in stored water volume (per unit ground area) per unit change in water potential [*Jones*, 1992]. For the purposes of equilibria and bifurcation analysis, the linearized components of the wood and leaf characteristic curve (or pressure-volume curve) are considered. This is akin to assuming hydraulic capacitances are constant. Also, xylem conductance is decreased by the most limiting water potential in the plant, i.e., ψ_l. With this assumption, the sensitivity of the modeled plant system to cavitation might be overestimated, but the fact that cavitation likely occurs first in the most distal parts (assuming homogeneous xylem properties) is accounted for. The water balance equation for the leaf compartment becomes

$$C_l \frac{d\psi_l}{dt} = E_{xl} - E = 2g_x(\psi_l)(\psi_x - \psi_l) - g_s(\psi_l)D, \quad (2)$$

where C_l is the leaf hydraulic capacitance. Evaporation from the stomatal pores is assumed to be driven by D—a justified assumption in canopies that are well coupled to the atmosphere that also allows a simpler comparison with ecophysiological studies that often report D only.

Once the conductances are defined, equations (1) and (2) and an additional continuity equation at the root node (i.e., $E_{sr} = E_{rx}$) provide a complete description of the three unknown water potentials in the storage pools and at the nodes. The soil-root conductance (g_{sr} in Figure 1) is modeled as the ratio of the soil hydraulic conductivity and a characteristic distance between the bulk soil and the roots representing the rhizosphere zone, which is in turn inversely related to the root area index [*Daly et al.*, 2004; *Manzoni et al.*, 2013b]. Accounting for root extension during dry periods, g_{sr} can be shown to approximately scale as $\approx \left(\psi_{s,sat}/\psi_s\right)^2$, where $\psi_{s,sat}$ is the soil water potential at saturation. This representation provides a simple relation between soil water availability and water transport to the roots that allows an analytical solution for the water potentials at all nodes in the soil-plant system [*Manzoni et al.*, 2014]. The xylem and stomatal conductances (g_x and g_s, respectively) are modeled as a function of the water potential in the corresponding compartment. For the liquid-phase conductances, the reduction occurring as water potentials become more negative is mainly due to cavitation [*Tyree and Sperry*, 1988]. Stomatal conductance is reduced at low water potentials partly because of developing pressure differences between epidermal and guard cells [*Buckley et al.*, 2003] and partly due to biochemical signals produced during soil and plant drying [*Tardieu and Davies*, 1993]. We do not distinguish between these two mechanisms but focus on the observed reduction in g_s as a function of leaf water potential during daytime. To retain analytical tractability, all conductances are assumed to decline linearly with declining leaf water potential and to be lower-bounded in magnitude to zero. The role of sigmoidal conductance-water potential relations is assessed in Appendix A. Based on these assumptions, the linear parts of the conductances are described by

$$g_x(\psi_l) = g_{x,max}\left(1 - \frac{1}{2}\frac{\psi_l}{\psi_{50,x}}\right), \quad (3)$$

$$g_s(\psi_l) = g_{s,max}\left(1 - \frac{1}{2}\frac{\psi_l}{\psi_{50,s}}\right), \quad (4)$$

where the subscript *max* indicates the conductances in saturated conditions and $\psi_{50,i}$ ($i = x, s$) represent the water potential levels at which each conductance is reduced by half. This simplified approach neglects uncontrolled water losses, e.g., through the leaf cuticle [*Kerstiens*, 1996]. To account for cuticular losses, the curve $E = g_s(\psi_l)D$ should flatten toward more negative water potentials instead of reaching zero with a discontinuity [*Boyer et al.*, 1997]. While this simplification does not alter the qualitative dynamics of the soil-plant system, it can affect the value of some equilibrium water potentials (Appendix A).

The maximum stomatal conductance is obtained from measured leaf area-specific conductance ($g^l_{s,max}$), multiplied by the leaf area index (LAI) to scale up to the ecosystem level (an approximation justified in

semiarid ecosystems with moderate LAI, while it might overestimate the canopy-level conductance in dense forests). The maximum xylem conductance is obtained from the sapwood-specific conductivity ($k^s_{s,max}$), multiplied by the sapwood area index (SAI) and divided by the canopy height (h)—a measure of the hydraulic pathway from the roots to the leaves [*Novick et al*., 2009; *Whitehead et al*., 1984].

During severe drought or frequent water stress cycles, the xylem hydraulic efficiency may deteriorate in a process typically referred to as "cavitation fatigue" [*Hacke et al*., 2001], which in turn causes declines in xylem hydraulic conductivity and makes the xylem more prone to cavitation by increasing $\psi_{50,x}$. Also, the attack by some pathogens and insects may cause similar damages to the xylem [*Domec et al*., 2013; *McDowell et al*., 2008] (although insects may also affect simultaneously the leaf area). To account for this deterioration, both $\psi_{50,x}$ and $g_{x,max}$ are multiplied by a factor $\xi < 1$ accounting for the long-term history of stress events. We do not model explicitly the stress events and the dynamics of recovery, since little is known about the mechanistic links between drought and hydraulic deterioration, and simply treat this stress factor as an empirical parameter. The goal of this analysis is to predict conditions in which hydraulic failure could develop assuming tissue deterioration has occurred, regardless of the specific cause (cavitation fatigue, pathogens, or insect damage).

3. Results

3.1. Overall Dynamic Behavior and Emergence of Hydraulic Failure

Figure 2a shows how leaf and xylem water potentials converge toward their stable equilibrium points when starting from a range of initial conditions. When stomatal closure occurs at water potentials less negative than full cavitation (i.e., $\psi_{50,s} > \psi_{50,x}$), the plant exhibits a "safe" behavior, with convergence of the water potentials toward a single, stable equilibrium point (blue line and blue filled circle in Figure 2a). As D increases and root water potential decreases, this stable equilibrium point shifts toward more negative water potential levels, but without qualitative changes (not shown). In contrast, when stomatal closure is delayed with respect to cavitation occurrence ($\psi_{50,s} < \psi_{50,x}$), a second, unstable equilibrium point emerges (black open circle in Figure 2a), giving rise to a prototypical saddle-node bifurcation. Under this scenario, some of the trajectories converge toward a third equilibrium point corresponding to the stable desiccated state. Importantly, the occurrence of the stable and unstable equilibrium points depends on environmental conditions. As shown in Figure 2a, dry conditions (high D as shown, or lowered ψ_r) may shift the nullclines of the system in such a way that the first two equilibrium points disappear and only a stable desiccated state remains (at $\psi_l = 2\psi_{50,s}$). This shift in dynamic behavior can serve as a pragmatic definition of "hydraulic failure."

3.2. Environmental Drivers of Hydraulic Failure

The equilibrium points of the leaf compartment are considered while employing ψ_r as a set boundary condition (and hence a control variable). Explicit dependence on soil water potential is considered in section 3.3. Assuming that the root ψ_r is known, the equilibrium points for the leaf water status can be computed by setting $d\psi_x/dt = 0$ in equation (1) (i.e., $\psi_x = (\psi_r + \psi_l)/2$) and $d\psi_l/dt = 0$ in equation (2) so that

$$\psi^*_{l,1;2} = \frac{\psi_r}{2} + \frac{\psi_{50,x}}{2}\left[2 - \chi \pm \sqrt{\left(\frac{\psi_r}{\psi_{50,x}}\right)^2 - 2(2+\chi)\frac{\psi_r}{\psi_{50,x}} + 8\chi\frac{\psi_{50,s}}{\psi_{50,x}} + (2-\chi)^2}\right], \qquad (5)$$

$$\psi^*_{l,3} = 2\psi_{50,s},$$

where $\chi = g_{s,max}D/\left(g_{x,max}\psi_{50,s}\right)$ is a nondimensional parameter group. When expressing the canopy-level conductances in terms of tissue-specific conductances and plant size, χ is obtained as $\chi = \left(g^l_{s,max}/k^s_{x,max}\right)(h\mathrm{LAI}/\mathrm{SAI})\left(D/\psi_{50,s}\right)$. Equation (5) depends on the *ratio* of the maximum conductances—not the individual magnitudes $g_{s,max}$ and $g_{x,max}$. The presence of three equilibrium points hints at the possibility of phase transitions as parameter values are altered. This type of behavior is the main feature of dynamical systems undergoing catastrophic phase transitions [*Zeeman*, 1976].

Figure 2b explores the origin of the equilibrium points, as intersections of the curve representing the water flux supplied to the leaves (E_{xl}) and the curve representing evaporation from the leaves (E). The biological

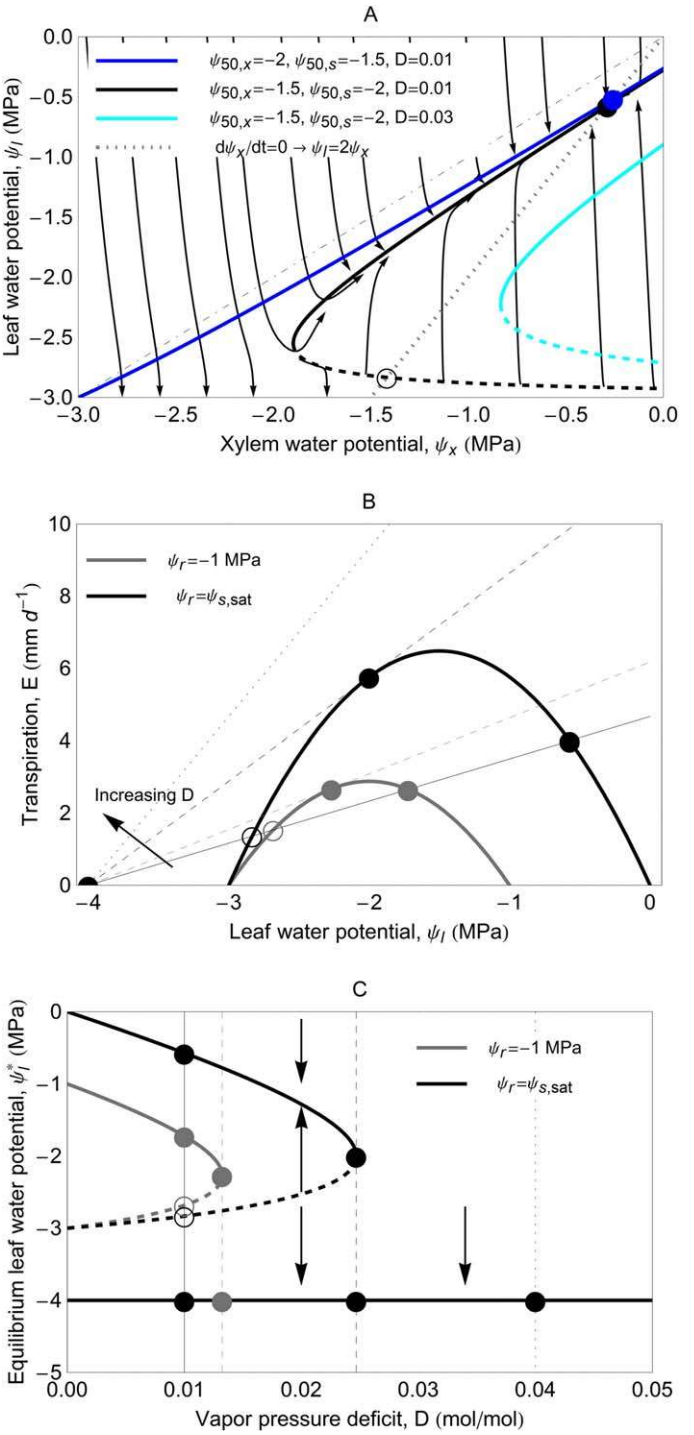

Figure 2. (a) Phase-space representation of the dynamics of stem (ψ_x) and leaf water potentials (ψ_l), and their equilibrium points, as hydraulic traits are varied from a "safe" plant (blue curve, $\psi_{50,s} > \psi_{50,x}$) to an "unsafe" plant (black and cyan curves, $\psi_{50,s} < \psi_{50,x}$). Thick curves represent the nullclines of the system (equilibrium points are located at their intersections), and thin arrows are streamlines illustrating the temporal evolution of ψ_x and ψ_l for the unsafe plant at low vapor pressure deficit (D); closed and open symbols, respectively, indicate stable and unstable equilibrium points. Note that only the nullcline corresponding to $d\psi_l/dt=0$ depends on hydraulic traits and D (solid and dashed thick curves), whereas the other nullcline corresponding to $d\psi_x/dt=0$ is simply given by $\psi_l=2\psi_x$ when $\psi_r \approx 0$ (dotted thick line). (b) Water supply to the leaves (thick curves), evaporative demand (thin curves), and equilibrium points at their intersections (circles) are shown as a function of ψ_l at different ψ_r (black versus gray) and D (solid lines for $D = 0.01$ mol mol^{-1}; dotted lines for $D = 0.04$ mol mol^{-1}; dashed lines for the D values at the transition to hydraulic failure at the two different ψ_r). (c) Equilibrium states as a function of D, for different ψ_r (as in Figure 2b). Thin vertical lines refer to the values of D also used in Figure 2b; arrows illustrate the direction of the leaf water potential trajectories. In all plots, $g_{s,max}$ =0.47 m d^{-1}, $g_{p,max}$ = 0.0086 m d^{-1} MPa^{-1}; ψ_r is set equal to the soil water potential at saturation, $\psi_{s,sat}$, except for gray curves in Figures 2b and 2c.

parameters ($\psi_{50,x}$, $\psi_{50,s}$, and $g_{s,max}/g_{x,max}$) are here kept constant, while the effects of different values of D and ψ_r are explored. The $\psi_{50,s}$ is chosen to be slightly more negative than $\psi_{50,x}$ thereby allowing the presence of an equilibrium point on the descending branch of the water supply curve. Higher vapor pressure deficit (increasing from solid to dashed and dotted thin lines) moves the evaporation curve upward, causing a shift from three equilibrium points to two (dashed lines) and eventually only the desiccated one at high D (dotted line). More negative values of ψ_r lower the water supply curve, thus also reducing the number of intersections from three to one. The effects of D and ψ_r are also shown in Figure 2c, where D is changed continuously on the abscissa.

The equilibrium points in the rising branch of the water supply curve (the least negative intersection of supply and demand in Figure 2b) are stable (solid symbols), whereas the equilibrium points on the descending branch are unstable (open symbols). The third equilibrium point at $\psi_l = 2\psi_{50,s}$ is also stable. This equilibrium point represents leaf desiccation, although it does not correspond to the atmospheric water potential due to the model simplifications (as explained in Appendix A). The stability of the equilibrium points can be assessed graphically from Figure 2b. When the water supply is larger than the evaporative demand, water potentials increase and hence, starting from a given ψ_l, the closer equilibrium points to the right is reached: this point attracts the dynamics and is stable. In contrast, when the evaporative demand is higher than the supply, ψ_l decreases and reaches the closer point to the left of the initial state. This is also a stable state, but it is characterized by desiccated conditions at $\psi_l = 2\psi_{50,s}$ if the initial condition is already a low ψ_l, or if the vapor pressure deficit is sufficiently high to allow only one or two equilibrium points (Figure 2c).

Had cuticular water losses been accounted for, the equilibrium points shown in Figure 2b would not have changed, except that the desiccated state would shift toward more negative water potential values, corresponding to the atmospheric water potential. In the case of a "safe" plant ($\psi_{50,s} > \psi_{50,x}$), the water potential value of the unstable equilibrium (where the supply curve reaches zero) would increase slightly because the demand curve flattens without reaching zero. For cuticular losses lower than 5% of the transpiration rate in well-watered conditions (a reasonable assumption [*Kerstiens*, 1996]), simulations under a wide range of soil water potentials and vapor pressure deficits show that the error in the calculated equilibrium water potential is smaller than 0.1 MPa in absolute value (not shown).

As shown in Figure 2, there are critical values of the parameters at which a regime shift occurs from a stable state that sustains transpiration and leaf functioning, to a single equilibrium point at leaf desiccation. These critical points mark the transition to hydraulic failure. Inspecting the mass balance of equation (2), it is possible to predict the type of dynamic transition that occurs at the critical point. Assuming steady state conditions for the xylem compartment so that $\psi_x = (\psi_l + \psi_r)/2$, it can be shown that the right hand side of equation (2) is a quadratic expression for the variable ψ_l. With a variable translation and recalling that C_l is assumed constant, this quadratic form can be recast into

$$\frac{d\phi}{dt} = \alpha + \beta\phi^2, \tag{6}$$

which recovers the canonical form of differential equations causing a *fold catastrophe*—the most primitive among the seven elementary catastrophes [*Thom*, 1975; *Zeeman*, 1976].

The transition points corresponding to the condition $\psi^*_{l,1} = \psi^*_{l,2}$ occur when the argument of the square root in equation (5) equals zero

$$\left(\frac{\psi_r}{\psi_{50,x}}\right)^2 - 2(2+\chi)\frac{\psi_r}{\psi_{50,x}} + 8\chi\frac{\psi_{50,s}}{\psi_{50,x}} + (2-\chi)^2 = 0. \tag{7}$$

Figure 3 explores the combinations of biological and environmental parameters at this critical point. As shown in Figure 3a, for given $\psi_{50,s}$ and $\psi_{50,x}$ (and for $\psi_{50,s} < \psi_{50,x}$), critical points occur only at certain combinations of D and root water potential. Combinations of D and ψ_r in the clear areas below the curves allow reaching a viable stable equilibrium (low D and high ψ_r); points above the curves in the shaded areas result in hydraulic failure (dry air and soil). As earlier noted, the critical points depend on the nondimensional group χ, with higher values of this ratio increasing evaporation with respect to water supply to the leaves, thus widening the range of environmental conditions triggering hydraulic failure. Recalling that

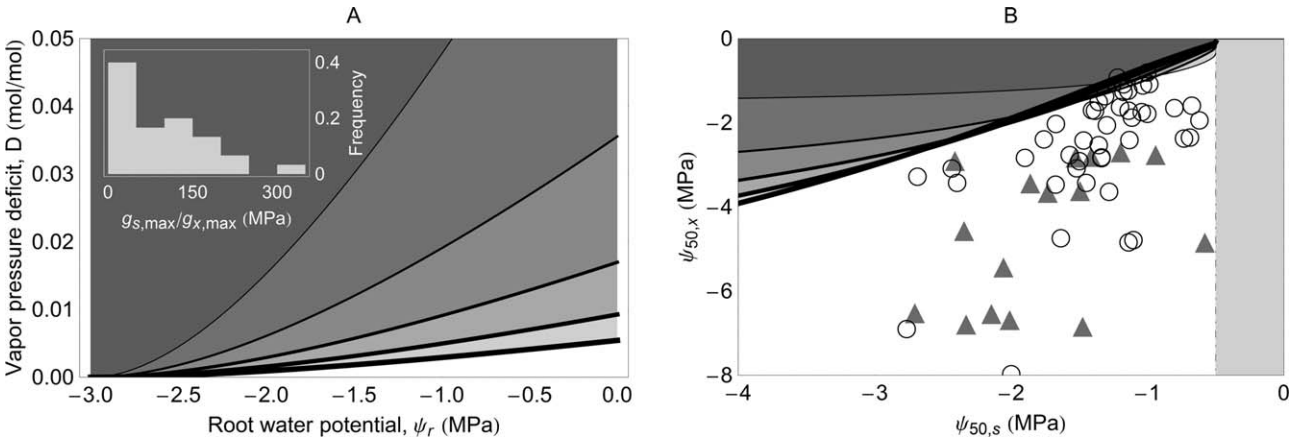

Figure 3. Combinations of environmental parameters triggering hydraulic failure (shaded areas). (a) Combinations of vapor pressure deficit (D) and root water potential (ψ_r), for different ratios of maximum stomatal conductance to maximum xylem conductance (from thin to thick lines: 5th, 25th, 50th, 75th, and 95th percentiles of $g_{s,max}/g_{x,max}$ based on data from *Novick et al*. [2009] and *Manzoni et al*. [2013b], see frequency plot in the inset) and for $\psi_{50,x} = -1.5$ MPa and $\psi_{50,s} = -2$ MPa. (b) Combinations of water potentials at 50% stomatal closure ($\psi_{50,s}$) and 50% loss of xylem conductance ($\psi_{50,x}$), for different levels of D (increasing from 0.01 to 0.06 mol mol^{-1} from thin to thick lines, for $g_{s,max}/g_{x,max} = 78$ MPa, i.e., the median of data point in Figure 3a); $\psi_r = -0.5$ MPa (dot-dashed vertical line). Symbols represent observed combinations of $\psi_{50,x}$ and $\psi_{50,s}$ in conifers (triangles) and angiosperms (circles) [*Manzoni et al*., 2014].

$\chi = \left(g^l_{s,max}/k^s_{x,max}\right)(h\mathrm{LAI}/\mathrm{SAI})\left(D/\psi_{50,s}\right)$, it becomes clear that different combinations of hydraulic traits ($g^l_{s,max}$, $k^s_{x,max}$, and $\psi_{50,s}$), plant morphology (SAI, LAI, and h), and environmental parameters (D) can equally satisfy equation (7). Therefore, coordination among hydraulic traits (e.g., $g^l_{s,max} \propto k^l_{x,max} = k^s_{x,max}\mathrm{SAI}/\mathrm{LAI}$) or among plant sizes (e.g., $\mathrm{LAI} \propto \mathrm{SAI}/h$) stabilizes χ.

Figure 3b shows combinations of $\psi_{50,s}$ and $\psi_{50,x}$ leading to hydraulic failure for a given ψ_r and varying D. When $\psi_{50,s}$ is less negative than $\psi_{50,x}$ only two equilibrium states occur: a stable state similar to the one shown in Figure 2b on the growing branch of the supply curve, and an unstable one at $\psi_l = 2\psi_{50,x}$. In this case, increasing D does not cause hydraulic failure. In contrast, when $\psi_{50,s} < \psi_{50,x}$ failure may occur and trait values permitting such occurrence widens as D is increased. Observed pairs of $\psi_{50,s}$ and $\psi_{50,x}$ appear to be in a relatively safe range, permitting leaves to remain hydrated unless ψ_r becomes more negative than the point of full stomatal closure (i.e., $\psi_r < 2\psi_{50,s}$). With reference to Figure 3b, lowering ψ_r shifts the vertical dot-dashed line leftward, thus extending the region of hydraulic failure to trait values that are otherwise deemed "safe." Notably, ψ_r decreases rapidly during soil drying due to a nonlinear dependence of soil hydraulic conductivity on soil moisture unless transpiration is reduced even more rapidly through stomatal closure (or leaf loss). Therefore, hydraulic failure could be driven by changes in soil hydraulic conductance, rather than cavitation per se—as earlier suggested [*Sperry et al*., 1998].

3.3. Hydraulic Damage by Cavitation Fatigue and Insect Infestations

The effects of hydraulic deterioration induced by either a history of water stress causing cavitation fatigue or insect damage are explored in Figure 4, in which the regions where stable and/or unstable equilibrium points occur are illustrated as a function of soil water potential and D. Two scenarios are considered in Figure 4: (i) constant hydraulic traits (as in previous sections) and (ii) decreasing hydraulic function by setting $\xi = 0.6$, i.e., xylem conductance and water potential at 50% cavitation (in absolute value) are reduced to 60% of their unstressed value. This value is representative of measured declines in hydraulic conductivity and $|\psi_{50,x}|$ in aspen (*Populus tremuloides*) following a severe drought [*Anderegg et al*., 2013]. When these hydraulic consequences of stress events and disturbance are accounted for, the moisture and D conditions triggering hydraulic failure become more widespread and the critical curve shifts toward moister conditions (red dashed curve). Hydraulically safe plants (as most species, see Figure 3) always exhibit a stable equilibrium point in the absence of cavitation fatigue, because $\psi_{50,s} > \psi_{50,x}$ (gray curves in Figure 4). However, as $\psi_{50,x}$ becomes less negative and the maximum xylem conductivity declines during a drought or after a sequence of dry/wetting cycles, hydraulic failure becomes possible even in these plants (black and red curves in Figure 4).

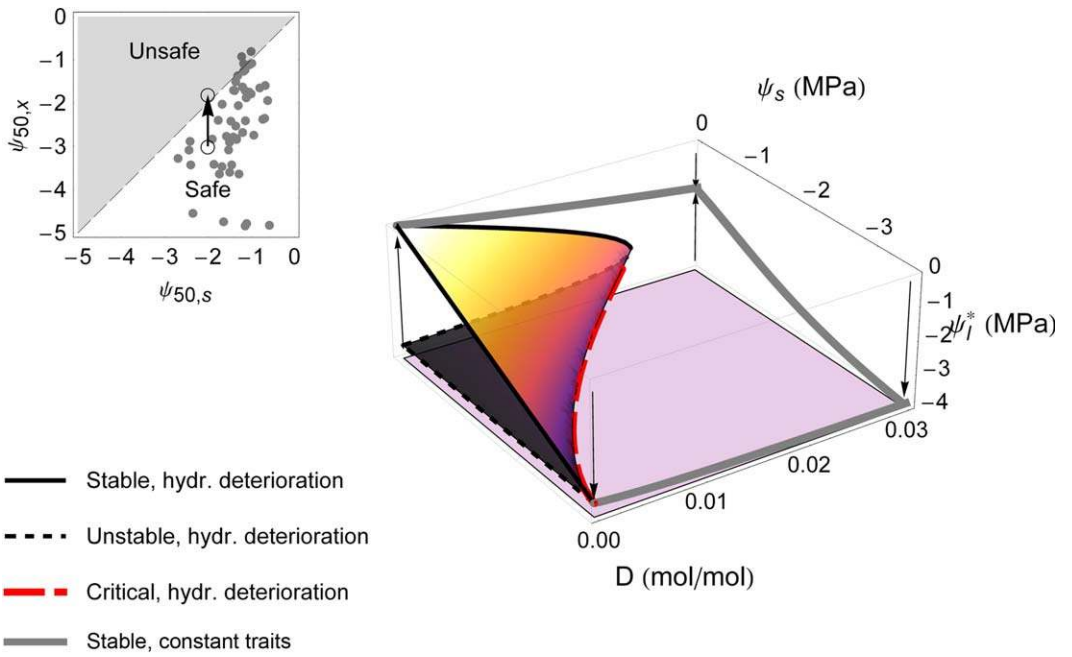

Figure 4. Combined effects of vapor pressure deficit (D) and soil water potential (ψ_s) on the leaf equilibrium points (ψ_l^*) when hydraulic deterioration is accounted for (black and red lines) or neglected (gray lines). Note that "safe" hydraulic traits (corresponding to gray lines) become "unsafe" (black lines) when xylem damage occurs. The red-dashed curve indicates the critical points at the onset of hydraulic failure; the light purple surface represents stable equilibrium points at desiccation ($\psi_l^* = 2\psi_{50,s}$). The inset compares the values of $\psi_{50,x}$ and $\psi_{50,s}$ used for the main plot (open circles with arrow indicating changes due to hydraulic deterioration) to observed values (as in Figure 3b); the shaded area in the inset refers to traits for which hydraulic failure may occur also in well-watered conditions.

4. Discussion

4.1. Comparison With Existing Plant Hydraulic Models

A minimal model of water flow in the soil-plant-atmosphere system was developed where the plant is described by two compartments (leaves and stem xylem) and a node for the roots (in instantaneous equilibrium), linked by hydraulic resistances (Figure 1). This model is similar to earlier ones that either neglected [*Magnani et al.*, 2002; *Steppe et al.*, 2006; *Whitehead et al.*, 1984] or explicitly considered the reduction of xylem conductance due to cavitation [*Daly et al.*, 2004; *Manzoni et al.*, 2013a; *Meyra et al.*, 2011]. More detailed discrete models [*Hölttä et al.*, 2009; *Sperry et al.*, 1998; *Tyree and Sperry*, 1988] and spatially explicit models [*Aumann and Ford*, 2002; *Bohrer et al.*, 2005] have also been developed. However, we opted for a minimal model whose simplicity allows obtaining analytical expressions for the dynamic transition to hydraulic failure.

Piecewise linear constitutive relations between conductances and water potentials (equations (3) and (4)) were employed to approximate the sigmoidal shape that these curves exhibit, especially in woody tissues [*Manzoni et al.*, 2013b; *Tyree and Sperry*, 1988]. Most plant hydraulic models adopt sigmoidal xylem vulnerability curves [*Bohrer et al.*, 2005; *Manzoni et al.*, 2013a; *Sperry et al.*, 1998] and stomatal response functions [e.g., *Jarvis*, 1976; *Tuzet et al.*, 2003]. Adopting such nonlinear shapes here would have hindered analytical tractability of this problem. To assess the sensitivity of the dynamic behavior (and the bifurcation type), we performed numerical analyses with sigmoidal curves (Appendix A). Employing sigmoidal response curves that gradually decline to zero as water potential becomes more negative introduces a plateau at high water potentials in the transpiration curves (thin solid lines in Figure 2b) and creates a range of possible intersections between demand and supply curve in dry conditions. While the first stable equilibrium point $\psi_{l,1}^*$ is not sensitive to the choice of the conductance curves, the number of the other equilibrium points is impacted, as shown in Appendix A.

Additionally, xylem conductivity was assumed homogeneous throughout the plant and sensitive to the water potential in the most distal parts (equation (3)) rather than to the mean xylem water potential. This

approximation leads to a conservative estimate of the critical conditions for hydraulic failure, thus reinforcing the conclusion that plants are relatively far from hydraulic dysfunction unless soil water potential nears the water potential at stomatal closure or hydraulic traits are deteriorated by previous stressing conditions. This conclusion would be further strengthened if leaf hydraulic failure acts as a safety fuse to protect the main stem from low water potential levels [*Brodribb and Cochard*, 2009; *Johnson et al*., 2011; *Zimmermann*, 1978]. In contrast, in species with vulnerable roots, hydraulic failure could occur earlier than predicted here. Accounting for changes in hydraulic traits from the roots to the leaves could allow a more precise definition of where cavitation occurs first [*Sperry et al*., 1998; *Tyree and Sperry*, 1988], at the expense of a more complex numerical approach that does not allow for analytical solutions.

4.2. Coordination of Hydraulic Traits to Avoid Hydraulic Failure

Leaf water potential changes diurnally depending on the balance of transpiration and water supply to the leaves. When transpiration is larger than the water supply, leaf water potential decreases until an equilibrium point is reached that balances inputs and outputs. Even in well-watered, conditions this equilibrium point may imply some degree of cavitation [*Manzoni et al*., 2013a]. Rapid stomatal closure compared to leaf conductance loss (i.e., $\psi_{50,s} > \psi_{50,x}$) allows the minimum leaf water potential to remain relatively far from hydraulic failure (Figure 3b). Low values of the ratio of plant-level stomatal to xylem conductance ($g_{s,max}/g_{x,max}$) also allow hydraulic operation in relatively dry conditions without incurring hydraulic failure (Figure 3a). When this ratio lowers, however, CO_2 uptake becomes inhibited, thus reducing carbon gains. A balance between these contrasting needs of avoiding hydraulic failure while maintaining carbon uptake is achieved by coordinating $g_{s,max}$ and $g_{x,max}$. Such coordination is evident in the positive correlation between maximum stomatal conductance ($g^l_{s,max}$) and xylem conductivity normalized by leaf area ($k^l_{x,max} = k^s_{x,max}\mathrm{SAI}/\mathrm{LAI}$) both across species and ecosystems [*Manzoni et al*., 2013b; *Mencuccini*, 2003] and during acclimation to altered environmental conditions [*Brodribb and Jordan*, 2011]. Reductions in $g_{s,max}$ caused by elevated atmospheric CO_2 concentrations [*Ainsworth and Rogers*, 2007] would tend to decrease χ for a given LAI and SAI, thereby increasing plant hydraulic safety. However, declines in stomatal conductance may be counterbalanced by increased LAI and the moisture threshold for stomatal closure may be insensitive to atmospheric CO_2, suggesting that a future CO_2-enriched atmosphere will not have an ameliorating effect on drought [*Duan et al*., 2014]. Also, decreasing the leaf area to sapwood area ratio along climatic gradients, and at a given site at both seasonal and ontogenetic scales may increase hydraulic safety [*Bucci et al*., 2006; *Magnani et al*., 2002; *Martinez-Vilalta et al*., 2009; *Maseda and Fernandez*, 2006]. Therefore, there are multiple avenues of hydraulic adjustment to improve gas exchange or protect from damages.

Being far from the tipping point leading to hydraulic failure, however, does not imply that the leaf water potential remains high. Rather, it means that even relatively negative water potentials are stable equilibrium points that are likely to be robust to small fluctuations in the environmental drivers (such as D). Steady state leaf and xylem water potentials can in fact be rather negative and cause significant levels of cavitation, but without leading to catastrophic hydraulic failures in most cases. Previous studies found that indeed transpiration is close, but lower than the critical value above which hydraulic failure occurs [*Hacke et al*., 2000; *Sperry et al*., 1998]. The results here (Figure 3b) are consistent with measured minimum leaf water potentials that in gymnosperms appear less negative than the water potential at 50% xylem cavitation, whereas in angiosperms these values are comparable [*Choat et al*., 2012; *Johnson et al*., 2012]. Partial cavitation can be considered "normal" during periods of intense transpiration, because water potential in the most distal parts of the plant necessarily decreases as transpiration increases [*Jones and Sutherland*, 1991; *Manzoni et al*., 2013a; *Nardini and Salleo*, 2000]. Moreover, declining water potentials in stem and branch xylem decrease the leaf water potential, thus triggering stomatal closure. Hence, partial cavitation may actually be instrumental to the prevention of hydraulic failure [*Nardini and Salleo*, 2000].

Assuming that the stomatal conductance declines with more negative water potentials leads to variable ψ_l, consistent with anisohydric behavior. In contrast, isohydric species close stomata to track changes in vapor pressure deficit and soil moisture and maintain a stable ψ_l [*McDowell et al*., 2008]. To model this behavior, a constant $\psi_l = \psi_{l,0}$ can be imposed (assuming $\psi_{l,0} > 2\psi_{50,x}$), thus inferring from equations (1) and (2) the rate of stomatal closure required to maintain $\psi_{l,0}$ as ψ_s declines. By doing so, the number of equilibrium solutions are reduced to a single stable point at $\psi_l = \psi_{l,0}$. The soil moisture level at which stomata are fully closed in isohydric species is thus easily obtained as $\psi_s = \psi_{l,0}$. More negative values of ψ_s do not cause

hydraulic failure because $\psi_{l,0} > 2\psi_{50,x}$, suggesting that perfectly isohydric species do not undergo hydraulic failure, but might be sensitive to dry conditions due to reduced gas exchange [*Plaut et al*., 2012]. It is also interesting to notice that imposing $\psi_l = \psi_{l,0}$ implies nearly linear scaling between liquid-phase and gas-phase conductances (results not shown), consistent with observed coordination between these traits at both tissue and whole-plant levels [*Manzoni et al*., 2013b; *Mencuccini*, 2003].

4.3. Xylem Damage, Risk of Hydraulic Failure, and Mortality

There is evidence that accumulated stresses during prolonged drought may lower the hydraulic efficiency and increase the sensitivity of plant xylem [*Anderegg et al*., 2013; *Hacke et al*., 2001; *Ogasa et al*., 2013]. Also, insect infestations may cause xylem damage when the insects mechanically damage the tissues [*McDowell et al*., 2008] or through indirect effects leading to lower xylem conductivity [*Domec et al*., 2013; *Hubbard et al*., 2013]. When the long-term deterioration of the xylem hydraulic properties is accounted for, plant status nears or crosses the threshold for hydraulic failure (Figure 4). If refilling of embolized tissues is not possible (e.g., because soil moisture does not improve), mortality caused by this accumulated hydraulic damage may ensue [*Anderegg et al*., 2013]. Even if hydraulic failure is prevented by stomatal closure, it has been suggested that the long-term reduction of CO_2 uptake may lead to depletion of carbohydrate reserves and eventually death by carbon starvation [*McDowell et al*., 2008; *Mitchell et al*., 2013; *Plaut et al*., 2012]. Clearly, to determine whether a plant undergoing hydraulic failure will actually die requires a far more complex model. Adding carbon dynamics to the hydraulic model would assist in disentangling catastrophic hydraulic failure from carbon starvation, but also the dynamics of refilling and recovery should be accounted for [*Brodribb et al*., 2010; *Brodribb and Cochard*, 2009; *Ogasa et al*., 2013; *Vesala et al*., 2003; *Zwieniecki and Holbrook*, 2009]. These additions would likely lead to hysteretic behavior in the water supply and demand curves, yielding even more complex dynamics.

4.4. Conclusions

Plant water relations are interpreted from a dynamical system perspective, showing that depending on environmental conditions the plant water status may reach one or two stable equilibrium points. At moderate vapor pressure deficit and high soil moisture, leaf water status equilibrates at values that allow plant functioning. However, at high vapor pressure deficit and low soil moisture, an alternative stable equilibrium point emerges corresponding to desiccation and thus catastrophic hydraulic failure. As environmental conditions are changed during a day (e.g., increasing D) or during a dry-down (decreasing soil moisture), the plant hydraulic system may fail, leading to desiccation. This abrupt transition is shown to be equivalent to a dynamic catastrophe (in the sense of *Thom* [1975]), providing a mathematical definition of plant hydraulic failure. The typical responses of stomatal conductance and xylem conductivity to changes in water potential, however, tend to ensure safe functioning even under drought. Only when prolonged stress or other disturbances deteriorate the hydraulic traits hydraulic failure becomes more likely. Linking this simple model to a plant carbon balance and describing the dynamics of recovery from xylem damage might provide further insights in the mechanisms leading to plant mortality.

Appendix A

Piecewise linear conductance-water potential relations have been assumed (equations (3) and (4)) to retain analytical tractability and ease the interpretation of the results. However, cavitation curves and stomatal closure curves often show a sigmoidal shape [*Manzoni et al*., 2013a; *Tuzet et al*., 2003] and can be modeled as

$$g_x(\psi_l) = g_{x,max}\left[1+\left(\frac{\psi_l}{\psi_{50,x}}\right)^{\alpha_x}\right]^{-1}, \tag{A1}$$

$$g_s(\psi_l) = g_{s,max}\left[1+\left(\frac{\psi_l}{\psi_{50,s}}\right)^{\alpha_s}\right]^{-1}, \tag{A2}$$

where the parameters α_x and α_s describe the shape of the curves. Larger values of these parameters yield more strongly sigmoidal shapes, in the limit leading to step functions decreasing from the maximum conductance values to zero at $\psi_l = \psi_{50,x}$ or $\psi_l = \psi_{50,s}$. Employing equations (A1) and (A2) does not allow

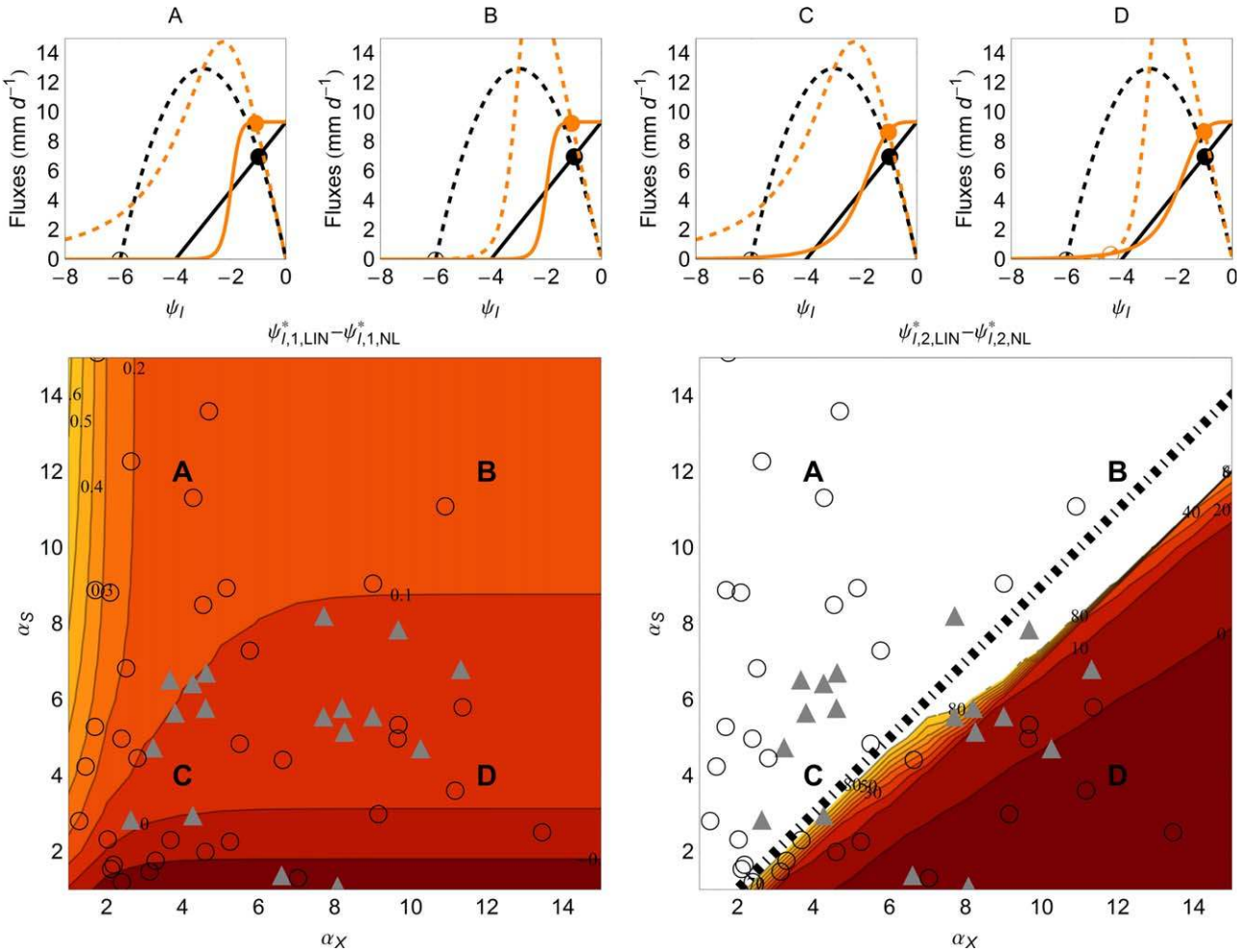

Figure A1. Comparison of equilibrium leaf water potentials computed using piecewise linear (equations (3) and (4)) and sigmoidal conductance-water potential relations (equations (A1) and (A2)). (top) Water supply (dashed) and demand (solid) curves for the piecewise linear (black curves) and the sigmoidal model (orange), with four combinations of shape parameters α_x and α_s (filled symbols: stable equilibrium points, open symbols: unstable equilibrium points). (bottom) Contour plots of the differences between equilibrium water potentials ψ_l^* computed using the piecewise linear (LIN) and the sigmoidal model (NL), as a function of α_x and α_s; uppercase letters refer to α_x and α_s employed in the top plots. The left and right plots refer to the stable and unstable equilibrium points, $\psi^*_{l,1}$ and $\psi^*_{l,2}$, respectively. The thick dot-dashed line separates combinations of α_x and α_s that allow only one (stable) equilibrium point ($\alpha_s > \alpha_x - 1$) from combinations allowing also an unstable equilibrium ($\alpha_s < \alpha_x - 1$). Open circles (angiosperms) and filled triangles (conifers) are obtained from published conductance-water potential data [*Manzoni et al.*, 2014]. In all plots, $\psi_r = 0$ MPa, $\psi_{50,x} = -3$ MPa, $\psi_{50,s} = -2$ MPa, $D = 0.02$ mol mol^{-1}, and other parameters are as in Figure 1.

obtaining analytical solutions for the equilibrium leaf water potential, except in a limited number of cases with integer values of the shape parameters. The α_x and α_s were estimated by nonlinear least squares fitting of cavitation and stomatal closure data [*Manzoni et al.*, 2014] obtaining a wide range of values (10th and 90th percentiles for α_x: 1.7 and 10.7, for α_s: 1.6 and 11.3, respectively).

Figure A1 shows that using piecewise linear curves does not alter significantly the values of the stable equilibrium water potential $\psi^*_{l,1}$, although it underestimates the corresponding transpiration rate. Errors associated to the unstable equilibrium point $\psi^*_{l,2}$ may be larger, due to the gradual decline of the sigmoidal curves toward zero (versus the sharp transition at $\psi_l = 2\psi_{50,x}$ and at $\psi_l = 2\psi_{50,s}$ using equations (3) and (4)). The estimated α_x and α_s values are overlapped to the contour plots in Figure A1 to show which errors are reasonable to expect based on the observed conductance curves.

The different shapes of equations (A1) and (A2) generate a richer dynamic behavior compared to the case of piecewise linear curves—ranging from zero to three equilibrium points (Figure A2). As the water potential tends to $-\infty$, the water supply curve tends to scale as $|\psi_l|^{1-\alpha_x}$ whereas the demand curve scales as $|\psi_l|^{-\alpha_s}$. Hence, when a first stable equilibrium occurs, a second, unstable equilibrium point also will occur as

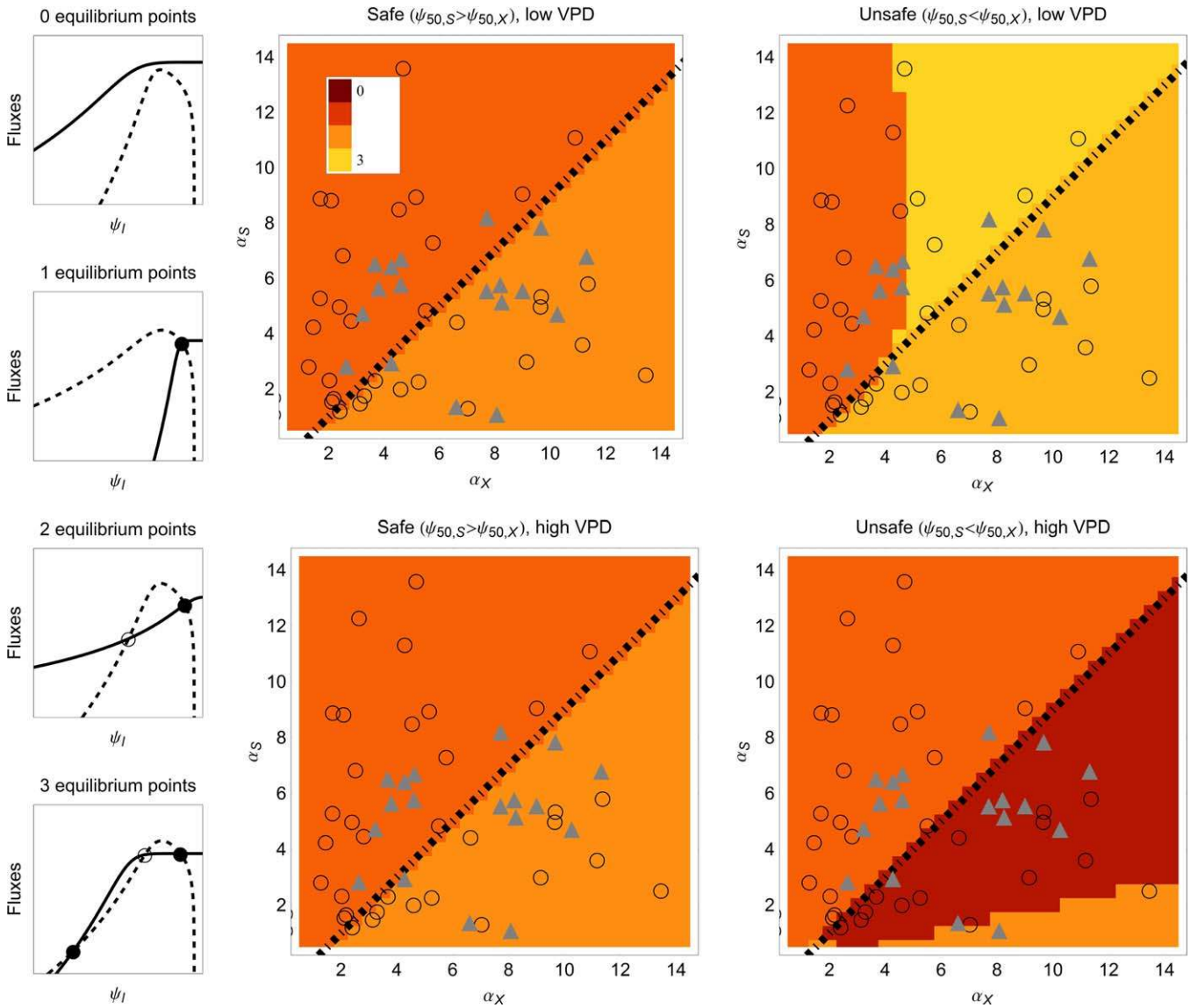

Figure A2. Main plots show number of equilibrium points as a function of α_x and α_s, indicated by different colors (see legend), and for different plant traits and vapor pressure deficit. Small plots on the left are examples illustrating how different shapes of supply (dashed) and demand (solid) curves (here in log-scale) yield different equilibrium points (filled symbols, stable equilibrium points; open symbols, unstable equilibrium points). Symbols and parameters are as in Figure A1, except $\psi_r = -0.5$ MPa.

long as the supply curve declines faster than the demand curve (i.e., $1-\alpha_x < -\alpha_s$, see dot-dashed lines in Figures A1 and A2). In such a case, there is no stable desiccation point at a finite value of ψ_l. In cases where two equilibrium points occur at relatively high water potentials, but $1-\alpha_x > -\alpha_s$, a third, stable equilibrium point also appears. This third equilibrium point corresponds to the desiccated state also defined by equation (5).

It is important to emphasize that in reality the stable desiccation point always exists, because as leaf water potential declines, so does the actual driving force of transpiration, i.e., the water vapor concentration difference between the stomatal cavity and the atmosphere. In fact, the vapor concentration in the stomatal cavity decreases from saturated levels at $\psi_l = 0$ (in such a case VPD is a good approximation of the "true" driving force) to lower values as ψ_l declines, eventually reaching the atmospheric water potential at complete desiccation [*Rodriguez-Iturbe and Porporato*, 2004, Chap. 4]. Therefore, our definition of desiccation point has to be interpreted in the context of the simplified model employed. Because the atmospheric water potential is one to two orders of magnitude lower than typical leaf water potentials, this

approximation of the driving force does not affect the leaf equilibrium points or the occurrence of hydraulic failure as described by the simplified model.

Acknowledgments
Plant trait data are available in the original cited publications or upon request to the first author. S.M. was supported by an excellence grant from the Faculty of Natural Resources and Agricultural Sciences, and the vice-chancellor of the Swedish University of Agricultural Sciences; the US DOE through the Office of Biological and Environmental Research, Terrestrial Carbon Processes program (DE-SC0006967), the Agriculture and Food Research Initiative from the USDA National Institute of Food and Agriculture (2011-67003-30222), the Binational Agricultural Research and Development (BARD) Fund (IS-4374-11C), and the National Science Foundation (FESD 1338694, CBET 1033467, EAR 1331846 for the Calhoun Critical Zone Observatory, and EAR 1316258) are also acknowledged. We also thank two reviewers and the Associate Editor for their constructive comments.

References

Ainsworth, E. A., and A. Rogers (2007), The response of photosynthesis and stomatal conductance to rising [CO_2]: Mechanisms and environmental interactions, *Plant Cell Environ.*, *30*(3), 258–270.
Allen, C. D., et al. (2010), A global overview of drought and heat-induced tree mortality reveals emerging climate change risks for forests, *For. Ecol. Manage.*, *259*(4), 660–684.
Anderegg, W. R. L., L. Plavcová, L. D. L. Anderegg, U. G. Hacke, J. A. Berry, and C. B. Field (2013), Drought's legacy: Multiyear hydraulic deterioration underlies widespread aspen forest die-off and portends increased future risk, *Global Change Biol.*, *19*, 1188–1196, doi:10.1111/gcb.12100.
Aumann, C. A., and E. D. Ford (2002), Modeling tree water flow as an unsaturated flow through a porous medium, *J. Theor. Biol.*, *219*(4), 415–429.
Bohrer, G., H. Mourad, T. A. Laursen, D. Drewry, R. Avissar, D. Poggi, R. Oren, and G. G. Katul (2005), Finite element tree crown hydrodynamics model (FETCH) using porous media flow within branching elements: A new representation of tree hydrodynamics, *Water Resour. Res.*, *41*, W11404, doi:10.1029/2005WR004181.
Boyer, J. S., S. C. Wong, and G. D. Farquhar (1997), CO_2 and water vapor exchange across leaf cuticle (epidermis) at various water potentials, *Plant Physiol.*, *114*(1), 185–191.
Brodribb, T. J., and H. Cochard (2009), Hydraulic failure defines the recovery and point of death in water-stressed conifers, *Plant Physiol.*, *149*(1), 575–584.
Brodribb, T. J., and G. J. Jordan (2011), Water supply and demand remain balanced during leaf acclimation of Nothofagus cunninghamii trees, *New Phytol.*, *192*(2), 437–448.
Brodribb, T. J., D. M. J. S. Bowman, S. Nichols, S. Delzon, and R. Burlett (2010), Xylem function and growth rate interact to determine recovery rates after exposure to extreme water deficit, *New Phytol.*, *188*(2), 533–542, doi:10.1111/j.1469–8137.2010.03393.x.
Bucci, S. J., F. G. Scholz, G. Goldstein, F. C. Meinzer, A. C. Franco, P. I. Campanello, R. Villalobos-Vega, M. Bustamante, and F. Miralles-Wilhelm (2006), Nutrient availability constrains the hydraulic architecture and water relations of savannah trees, *Plant Cell Environ.*, *29*(12), 2153–2167.
Buckley, T. N. (2005), The control of stomata by water balance, *New Phytol.*, *168*(2), 275–291.
Buckley, T. N., K. A. Mott, and G. D. Farquhar (2003), A hydromechanical and biochemical model of stomatal conductance, *Plant Cell Environ.*, *26*(10), 1767–1785.
Choat, B., et al. (2012), Global convergence in the vulnerability of forests to drought, *Nature*, *491*, 752–755, doi:10.1038/nature11688.
Daly, E., A. Porporato, and I. Rodriguez-Iturbe (2004), Coupled dynamics of photosynthesis, transpiration, and soil water balance. Part I: Upscaling from hourly to daily level, *J. Hydrometeorol.*, *5*(3), 546–558.
Domec, J.-C., L. N. Rivera, J. S. King, I. Peszlen, F. Hain, B. Smith, and J. Frampton (2013), Hemlock woolly adelgid (Adelges tsugae) infestation affects water and carbon relations of eastern hemlock (Tsuga canadensis) and Carolina hemlock (Tsuga caroliniana), *New Phytol.*, *199*(2), 452–463, doi:10.1111/nph.12263.
Duan, H., R. A. Duursma, G. Huang, R. A. Smith, B. Choat, A. P. O'Grady, and D. T. Tissue (2014), Elevated [CO_2] does not ameliorate the negative effects of elevated temperature on drought-induced mortality in Eucalyptus radiata seedlings, *Plant Cell Environ.*, *37*(7), 1598–1613, doi:10.1111/pce.12260.
Hacke, U. G., J. S. Sperry, B. E. Ewers, D. S. Ellsworth, K. V. R. Schafer, and R. Oren (2000), Influence of soil porosity on water use in *Pinus taeda*, *Oecologia*, *124*(4), 495–505.
Hacke, U. G., V. Stiller, J. S. Sperry, J. Pittermann, and K. A. McCulloh (2001), Cavitation fatigue. Embolism and refilling cycles can weaken the cavitation resistance of xylem, *Plant Physiol.*, *125*(2), 779–786, doi:10.1104/pp.125.2.779.
Hölttä, T., H. Cochard, E. Nikinmaa, and M. Mencuccini (2009), Capacitive effect of cavitation in xylem conduits: Results from a dynamic model, *Plant Cell Environ.*, *32*(1), 10–21.
Hubbard, R. M., C. C. Rhoades, K. Elder, and J. Negron (2013), Changes in transpiration and foliage growth in lodgepole pine trees following mountain pine beetle attack and mechanical girdling, *For. Ecol. Manage.*, *289*, 312–317, doi:10.1016/j.foreco.2012.09.028.
Jarvis, P. G. (1976), Interpretation of variations in leaf water potential and stomatal conductance found in canopies in field, *Philos. Trans. R. Soc. London B*, *273*(927), 593–610.
Johnson, D. M., K. A. McCulloh, F. C. Meinzer, D. R. Woodruff, and D. M. Eissenstat (2011), Hydraulic patterns and safety margins, from stem to stomata, in three eastern US tree species, *Tree Physiol.*, *31*(6), 659–668.
Johnson, D. M., K. A. McCulloch, D. R. Woodruff, and F. C. Meinzer (2012), Hydraulic safety margins and embolism reversal in stems and leaves: Why are conifers and angiosperms so different?, *Plant Sci.*, *195*, 48–53.
Jones, H. G. (1992), *Plants and Microclimate. A Quantitative Approach to Environmental Plant Physiology*, 428 pp., Cambridge Univ. Press, Cambridge, New York.
Jones, H. G., and R. A. Sutherland (1991), Stomatal control of xylem embolism, *Plant Cell Environ.*, *14*(6), 607–612.
Kerstiens, G. (1996), Cuticular water permeability and its physiological significance, *J. Exp. Bot.*, *47*(305), 1813–1832.
Magnani, F., J. Grace, and M. Borghetti (2002), Adjustment of tree structure in response to the environment under hydraulic constraints, *Funct. Ecol.*, *16*(3), 385–393, doi:10.1046/j.1365–2435.2002.00630.x.
Manzoni, S., G. Vico, G. Katul, S. Palmroth, R. B. Jackson, and A. Porporato (2013a), Hydraulic limits on maximum plant transpiration and the origin of the safety-efficiency tradeoff, *New Phytol.*, *198*(1), 169–178.
Manzoni, S., G. Vico, G. Katul, and A. Porporato (2013b), Biological constraints on water transport in the soil-plant-atmosphere system, *Adv. Water Resour.*, *51*, 292–304.
Manzoni, S., G. Vico, G. Katul, S. Palmroth, and A. Porporato (2014), Optimal plant water-use strategies under stochastic rainfall, *Water Resour. Res.*, *50*, doi:10.1002/2014WR015375.
Martinez-Vilalta, J., and J. Pinol (2002), Drought-induced mortality and hydraulic architecture in pine populations of the NE Iberian Peninsula, *For. Ecol. Manage.*, *161*(1–3), 247–256.
Martinez-Vilalta, J., et al. (2009), Hydraulic adjustment of Scots pine across Europe, *New Phytol.*, *184*(2), 353–364.
Maseda, P. H., and R. J. Fernandez (2006), Stay wet or else: Three ways in which plants can adjust hydraulically to their environment, *J. Exp. Bot.*, *57*(15), 3963–3977.

McDowell, N., et al. (2008), Mechanisms of plant survival and mortality during drought: Why do some plants survive while others succumb to drought?, *New Phytol.*, *178*(4), 719–739.
Meinzer, F. C., D. R. Woodruff, J. C. Domec, G. Goldstein, P. I. Campanello, M. G. Gatti, and R. Villalobos-Vega (2008), Coordination of leaf and stem water transport properties in tropical forest trees, *Oecologia*, *156*(1), 31–41.
Mencuccini, M. (2003), The ecological significance of long-distance water transport: Short-term regulation, long-term acclimation and the hydraulic costs of stature across plant life forms, *Plant Cell Environ.*, *26*(1), 163–182.
Meyra, A. G., G. J. Zarragoicoechea, and V. A. Kuz (2011), A similarity law in botanic. The case of hydraulic conductivity of trees, *Eur. Phys. J. D*, *62*(1), 19–23.
Mitchell, P. J., A. P. O'Grady, D. T. Tissue, D. A. White, M. L. Ottenschlaeger, and E. A. Pinkard (2013), Drought response strategies define the relative contributions of hydraulic dysfunction and carbohydrate depletion during tree mortality, *New Phytol.*, *197*(3), 862–872, doi: 10.1111/nph.12064.
Nardini, A., and S. Salleo (2000), Limitation of stomatal conductance by hydraulic traits: Sensing or preventing xylem cavitation?, *Trees Struct. Funct.*, *15*(1), 14–24.
Novick, K., R. Oren, P. Stoy, J. Y. Juang, M. Siqueira, and G. Katul (2009), The relationship between reference canopy conductance and simplified hydraulic architecture, *Adv. Water Resour.*, *32*(6), 809–819.
Ogasa, M., N. H. Miki, Y. Murakami, and K. Yoshikawa (2013), Recovery performance in xylem hydraulic conductivity is correlated with cavitation resistance for temperate deciduous tree species, *Tree Physiol.*, *33*(4), 335–344, doi:10.1093/treephys/tpt010.
Plaut, J. A., E. A. Yepez, J. Hill, R. Pangle, J. S. Sperry, W. T. Pockman, and N. G. McDowell (2012), Hydraulic limits preceding mortality in a pinon-juniper woodland under experimental drought, *Plant Cell Environ.*, *35*(9), 1601–1617, doi:10.1111/j.1365–3040.2012.02512.x.
Rodriguez-Iturbe, I., and A. Porporato (2004), *Ecohydrology of Water-Controlled Ecosystems. Soil Moisture and Plant Dynamics*, Cambridge Univ. Press, Cambridge, U. K.
Runyan, C. W., P. D'Odorico, and D. Lawrence (2012), Physical and biological feedbacks of deforestation, *Rev. Geophys.*, *50*, RG4006, doi: 10.1029/2012rg000394.
Scheffer, M., S. Carpenter, J. A. Foley, C. Folke, and B. Walker (2001), Catastrophic shifts in ecosystems, *Nature*, *413*(6856), 591–596.
Sperry, J. S., F. R. Adler, G. S. Campbell, and J. P. Comstock (1998), Limitation of plant water use by rhizosphere and xylem conductance: Results from a model, *Plant Cell Environ.*, *21*(4), 347–359.
Steppe, K., D. J. W. De Pauw, R. Lemeur, and P. A. Vanrolleghem (2006), A mathematical model linking tree sap flow dynamics to daily stem diameter fluctuations and radial stem growth, *Tree Physiol.*, *26*(3), 257–273.
Tardieu, F., and W. J. Davies (1993), Integration of hydraulic and chemical signaling in the control of stomatal conductance and water status of droughted plants, *Plant Cell Environ.*, *16*(4), 341–349.
Thom, R. (1975), *Structural Stability and Morphogenesis; An Outline of a General Theory of Models*, 348 pp., Benjamin, Reading, Mass.
Tuzet, A., A. Perrier, and R. Leuning (2003), A coupled model of stomatal conductance, photosynthesis and transpiration, *Plant Cell Environ.*, *26*(7), 1097–1116.
Tyree, M. T., and J. S. Sperry (1988), Do woody-plants operate near the point of catastrophic xylem dysfunction caused by dynamic water-stress—Answers from a model, *Plant Physiol.*, *88*(3), 574–580.
van den Honert, T. H. (1948), Water transport in plants as a catenary process, *Discuss. Faraday Soc.*, *3*, 146–153.
Vesala, T., T. Hölttä, M. Peramaki, and E. Nikinmaa (2003), Refilling of a hydraulically isolated embolized xylem vessel: Model calculations, *Ann. Bot.*, *91*(4), 419–428, doi:10.1093/aob/mcg022.
Whitehead, D., W. R. N. Edwards, and P. G. Jarvis (1984), Conducting sapwood area, foliage area, and permeability in mature trees of *Picea sitchensis* and *Pinus contorta*, *Can. J. For. Res.*, *14*(6), 940–947, doi:10.1139/x84–166.
Zeeman, E. C. (1976), Catastrophe theory, *Sci. Am.*, *234*(4), 65–83.
Zimmermann, M. H. (1978), Hydraulic architecture of some diffuse-porous trees, *Can. J. Bot.*, *56*(18), 2286–2295.
Zwieniecki, M. A., and N. M. Holbrook (2009), Confronting Maxwell's demon: Biophysics of xylem embolism repair, *Trends Plant Sci.*, *14*(10), 530–534.